TTK/MPS1 inhibitor OSU-13 targets the mitotic checkpoint and is a potential therapeutic strategy for myeloma

Larissa Valle Guilhen Longo,[1,2] Tiffany Hughes,[1,2] Betina McNeil-Laidley,[1,2] Francesca Cottini,[1,2] Gerard Hilinski,[3] Elizabeth Merritt[2] and Don M. Benson Jr.[1,2]

[1]Division of Hematology, Department of Internal Medicine, Ohio State University; [2]Comprehensive Cancer Center and James Cancer Hospital and Solove Research Institute and [3]Drug Development Institute, Comprehensive Cancer Center, James Cancer Hospital and Solove Research Institute, Columbus, OH, USA

Correspondence: D.M. Benson
Don.Benson@osumc.edu

Received: January 27, 2023.
Accepted: July 20, 2023.
Early view: July 27, 2023.

https://doi.org/10.3324/haematol.2023.282838

Abstract

Despite substantial recent advances in treatment, multiple myeloma (MM) remains an incurable disease, with a shortage of treatment options for patients with high-risk disease, warranting the need for novel therapeutic targets and treatment approaches. Threonine and tyrosine kinase (TTK), also known as monopolar spindle 1 (MPS1), is a kinase essential for the mitotic spindle checkpoint whose expression correlates to unfavorable prognosis in several cancers. Here, we report the importance of TTK in MM, and the effects of the TTK inhibitor OSU-13. Elevated *TTK* expression correlated with amplification/gain of 1q21 and decreased overall and event-free survival in MM. Treatment with OSU-13 inhibited TTK activity efficiently and selectively at a similar concentration range to other TTK inhibitor clinical candidates. OSU-13 reduced proliferation and viability of primary human MM cells and cell lines, especially those with high 1q21 copy numbers, and triggered apoptosis through caspase 3 and 7 activation. In addition, OSU-13 induced DNA damage and severe defects in chromosome alignment and segregation, generating aneuploidy. *In vivo*, OSU-13 decreased tumor growth in mice with NCI-H929 xenografts. Collectively, our findings reveal that inhibiting TTK with OSU-13 is a potential therapeutic strategy for MM, particularly for a subset of high-risk patients with poor outcome.

Introduction

Multiple myeloma (MM) is a plasma cell disorder that accounts for more than 10% of hematologic cancers.[1] Despite the recent improvement in overall survival of patients with MM due to novel treatment options,[2,3] MM is still a mostly incurable cancer,[4] warranting the need for novel therapeutic targets, especially for patients with high-risk disease.

The presence of genetic alterations is an important hallmark of cancer.[5,6] In MM, structural and numerical genetic abnormalities are usually associated with disease development and progression.[7] Aneuploidy is present in about 70% of MM cases.[8] In addition, deletions, duplications, or translocations are very common events in MM,[9,10] some of which - t(4;14)(p16;q32), t(14;16)(q32;q23), and del(17p) - are considered poor prognostic indicators.[11] Possible mechanisms leading to genomic instability in MM include elevated homologous recombination activity, which causes an increased mutation rate and accumulation of genetic variation,[12] and centrosome amplification, which is frequent in MM and has been associated with high-risk disease and poor prognosis.[13]

Adequate chromosome segregation is essential for genomic stability and relies on a group of proteins known as the spindle assembly checkpoint (SAC).[14] The SAC blocks cell cycle progression until the chromosomes are correctly attached to the spindle microtubules.[15] Failure of this process can cause uneven chromosomal segregation and aneuploidy, resulting in chromosomal instability.[16] Manipulation of SAC proteins leads to tumor formation in animal models.[17,18] Accordingly, drugs that interfere with SAC, such as inhibitors of Aurora kinases, Polo-like kinases, CENP-E, and threonine and tyrosine kinase (TTK) have been investigated or are being tested in clinical trials for several cancers including MM.[19-21]

TTK, also known as monopolar spindle 1 (MPS1), participates in the regulation of the DNA damage checkpoint response,[22] centrosome duplication,[23] and mitosis arrest until proper chromosome alignment, playing an essential role in SAC.[24] High levels of *TTK* expression correlate to unfavorable prognosis in several cancers,[25-27] and TTK inhibition shows

potential utility for the treatment of glioma,[28] melanoma,[29] and colon,[30] breast,[31,32] lung,[32] ovarian,[29,32] and cervical[33] cancers. Consequently, many clinical trials have tested TTK inhibitors - either as monotherapy or combinations - for the treatment of solid tumors, especially breast cancer. However, to date, there have been no clinical trials with TTK inhibitors involving patients with any kind of hematologic malignancies.

In 2017, the TTK/MPS1 inhibitor OSU-13 was identified as a potential therapy for breast cancer.[31] Here, we provide new data establishing the relevance of *TTK* expression in MM prognosis and perform the first comprehensive study using a TTK/MPS1 inhibitor as a therapeutic strategy for a hematologic malignancy.

Methods

OSU-13 drug

OSU-13 was provided by the Drug Development Institute of the Ohio State University and stored at -20°C at 10 mM in dimethyl sulfoxide (DMSO).

Prognostic survival analysis

Overall survival and event-free survival outcome studies were performed in 769 patients using the GSE2658 dataset. The median value of *TTK* levels was used as a cut-off to define patients with low (n=386) or high (n=383) *TTK* expression. Prognostic value of *TTK* was evaluated by the Kaplan-Meier curve, obtained from www.canevolve.org. TTK expression analysis in high-risk MM with specific genetic alterations (17p del, t(4;14), t(11;14), t(8;14), and 1q21 gain) was performed in the MMRF CoMMpass database.

Viability, apoptosis and necroptosis assays

For viability measurement, cells were plated at 100,000 cells/mL in medium containing DMSO or 0.5 μM OSU-13 and incubated for 24, 48, and 72 hours (h) at 37°C and 5% CO_2. Afterwards, cells were stained with Zombie-aqua (Life Technologies; Carlsbad, CA, USA) according to manufacturer's instructions. Cells were then analyzed using an Attune Nxt cytometer (Invitrogen; Waltham, MA, USA), and FlowJo software (FlowJo LLC; Ashland, OR, USA).

For apoptosis and necroptosis inhibition assays, OPM-2 cells (250,000 cells/mL) were pre-incubated for 1 h at 37°C in medium containing 100 μM of the general caspase inhibitor Z-VAD-FMK (Sigma-Aldrich; St Louis, MO, USA) or the necroptosis inhibitor necrostatin-1s (Cell Signaling Inc.; Danvers, MA, USA). Then, cells were washed and incubated for 72 h in medium containing DMSO or 1 μM OSU-13, stained with Zombie-aqua (Life Technologies), and cell viability was assessed as previously described.

Fluorescence microscopy of chromosome segregation

OPM-2 cells ($1x10^6$) were synchronized at G1/S by double thymidine block. Cells were incubated for 16 h in medium containing 2 mM thymidine (Sigma-Aldrich), released for 8 h in fresh medium, and incubated in 2 mM thymidine for additional 16 h. Next, cells were washed, and cell cycle release was induced with 24 μM 2'-deoxycytidine (Sigma-Aldrich) plus DMSO or 1 μM OSU-13 for 9 h. Cells were resuspended in 100 μL phosphate-buffered saline (PBS), immobilized onto a microscope slide using a Cytospin (Thermo Fisher Scientific; Waltham, MA, USA), mounted with Prolong Glass Antifade Mountant with NucBlue (Thermo Fisher Scientific), and imaged using a Nikon DM5000 B microscope (Tokyo, Japan) equipped with fluorescence optics with a Leica X63 oil immersion objective (Wetzlar, Germany). Images were analyzed using ImageJ (NIH; Bethesda, MD, USA), and the percentage of anaphase and telophase cells with and without lagging chromosomes was manually calculated.

Statistical considerations

Unless specified otherwise, all data are presented as mean values ± standard deviation (SD) from independent experiments. Student's *t* test was used to evaluate differences between conditions with *P* value <0.05 considered to be statistically significant. $^{*}P<0.05$, $^{**}P<0.01$, $^{***}P<0.001$ and $^{****}P<0.0001$. The correlation between sensitivity to OSU-13 and 1q21 copy number in the cell lines was analyzed using the non-parametric Spearman's rank correlation coefficient.

Additional methods

Cell lines, primary cell experiments, small interfering RNA (siRNA) knockdown, real-time polymerase chain reaction (PCR), NanoBRET™, kinase profiling, co-crystallization, cell viability and proliferation assays, caspases 3 and 7 activity assay, western blotting, TUNEL, cell cycle analysis, metaphase chromosome spread, and studies in murine model are described in the *Online Supplementary Appendix*. Experiments involving human subject samples were conducted with the approval of The Ohio State University Institutional Review Board (IRB 2023C0065).

Results

TTK expression correlates with multiple myeloma prognosis and plays a role in the survival of multiple myeloma cell lines

High *TTK* expression correlates to unfavorable prognosis in several cancers.[25-28,34] In order to determine the relevance of *TTK* expression in MM prognosis, we examined the GSE2658 dataset and the CoMMpass database, analyzing the association of *TTK* expression with clinical outcome and chromosomal alterations in MM patients (n=769). We found that elevated *TTK* expression correlated with decreased overall ($P=0.0001$) and event-free ($P<0.0001$) survival (Figure 1A, B). Furthermore, *TTK* expression was higher in patients

with amplification or gain of 1q21, a genetic alteration found in high-risk MM (P<0.0001) (Figure 1C). No correlation was seen between *TTK* expression and other high-risk genetic alterations, such as deletion of 17p or t(4;14), t(8;14), or t(11;14) translocations (*Online Supplementary Figure S1*).

We also compared *TTK* expression levels in eight human MM cell lines and primary CD138$^+$ plasma cells isolated from bone marrow (BM) of four recently diagnosed, untreated MM patients (Figure 1D). MM cell lines exhibited higher *TTK* expression than primary CD138$^+$ cells. MM.1S showed the highest expression (16.2-fold higher than CD138$^+$ cells), whereas L363 had the lowest expression (3.2-fold increase). In order to investigate the role of *TTK* in MM cell lines, we specifically knocked down *TTK* expression in OPM-2 and NCI-H929 using Alexa Fluor 647-conjugated non-targeting scrambled or *TTK*-specific siRNA (*Online Supplementary Figure S2*). Streptolysin was used to facilitate siRNA uptake, and cell viability was evaluated using Zombie Aqua

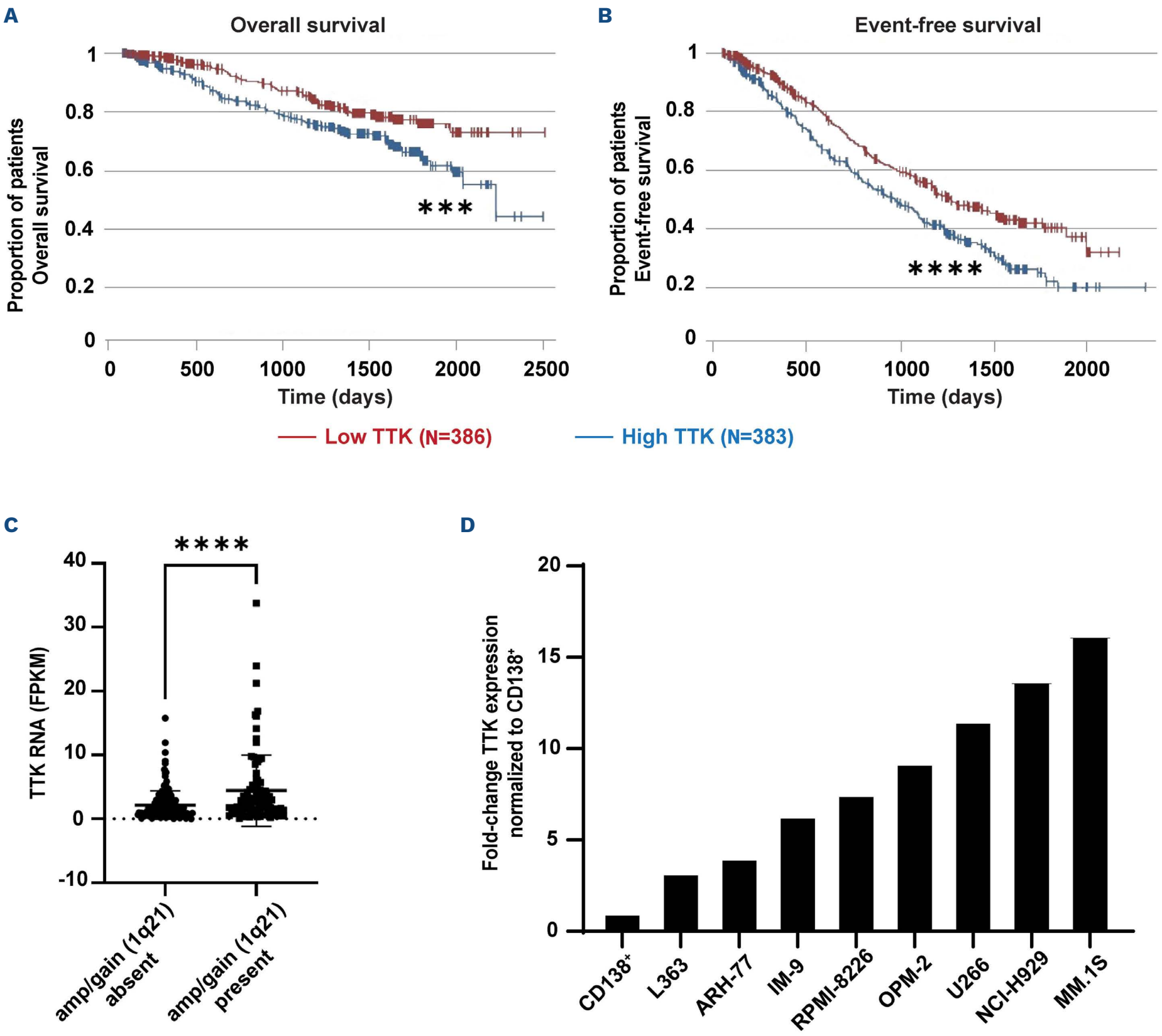

Figure 1 *TTK* expression correlates with multiple myeloma prognosis and varies in human multiple myeloma cell lines. (A) Overall and (B) event-free survival outcome studies from GSE2658 dataset. Median value of *TTK* levels were used as a cut-off to define "low *TTK*" and "high *TTK*" patients. Kaplan Meier curves were obtained from www.canevolve.org; ***P<0.001; ****P<0.0001. (C) Analysis from MMRF CoMMpass database of the *TTK* expression in multiple myeloma (MM) patients with (N=99) or without +1q21 (N=171); ****P<0.0001. (D) *TTK* expression in human MM cell lines. Values were normalized to the average of *TTK* expression in CD138$^+$ cells from four patients with MM. FPKM: fragments per kilobase per million.

staining. Knock-down of *TTK* was confirmed by quantitative PCR (*data not shown*). Our results exhibited a significant decrease in viability in *TTK*-siRNA$^+$ cells compared to cells transfected with non-targeting scrambled siRNA in both cell lines, with a more pronounced effect in NCI-H929. Following treatment with 20 units (U) of streptolysin, 51±5.8% of *TTK*-siRNA$^+$ NCI-H929 cells were dead (Zombie$^+$), in contrast to only 16±6.2% of scrambled siRNA$^+$ cells (P<0.001). These findings highlight the critical role of TTK in MM cell survival and suggest that targeting TTK could serve as a potential therapeutic strategy for MM.

OSU-13 efficiently and selectively inhibits TTK

In order to analyze the interaction between TTK and its novel small molecule inhibitor OSU-13, their co-crystal structure was obtained at a 2.37 Å resolution (Figure 2A). We determined that OSU-13 binds to the ATP-binding pocket, forming multiple interactions with the protein kinase hinge region, P-loop, and A-loop. OSU-13 inserts between Val539, Ala551 and Ile531 on one side and Leu654, Ile663 and Ile586 on the other, as well as the gatekeeper residue Met602 thiol deep in the pocket. The pyrrolopyrimidine bicyclic scaffold donates a H-bond to the Glu603 main chain carbonyl oxygen and accepts a H-bond from the Gly605 amide nitrogen. Additionally, OSU-13 forms a H-bond with the Gly605 main chain carbonyl oxygen and establishes van der Waals contacts with the ribose-binding pocket and the solvent-exposed channel.

OSU-13's activity was initially measured by a TTK target engagement assay (NanoBRET™). We compared its relative

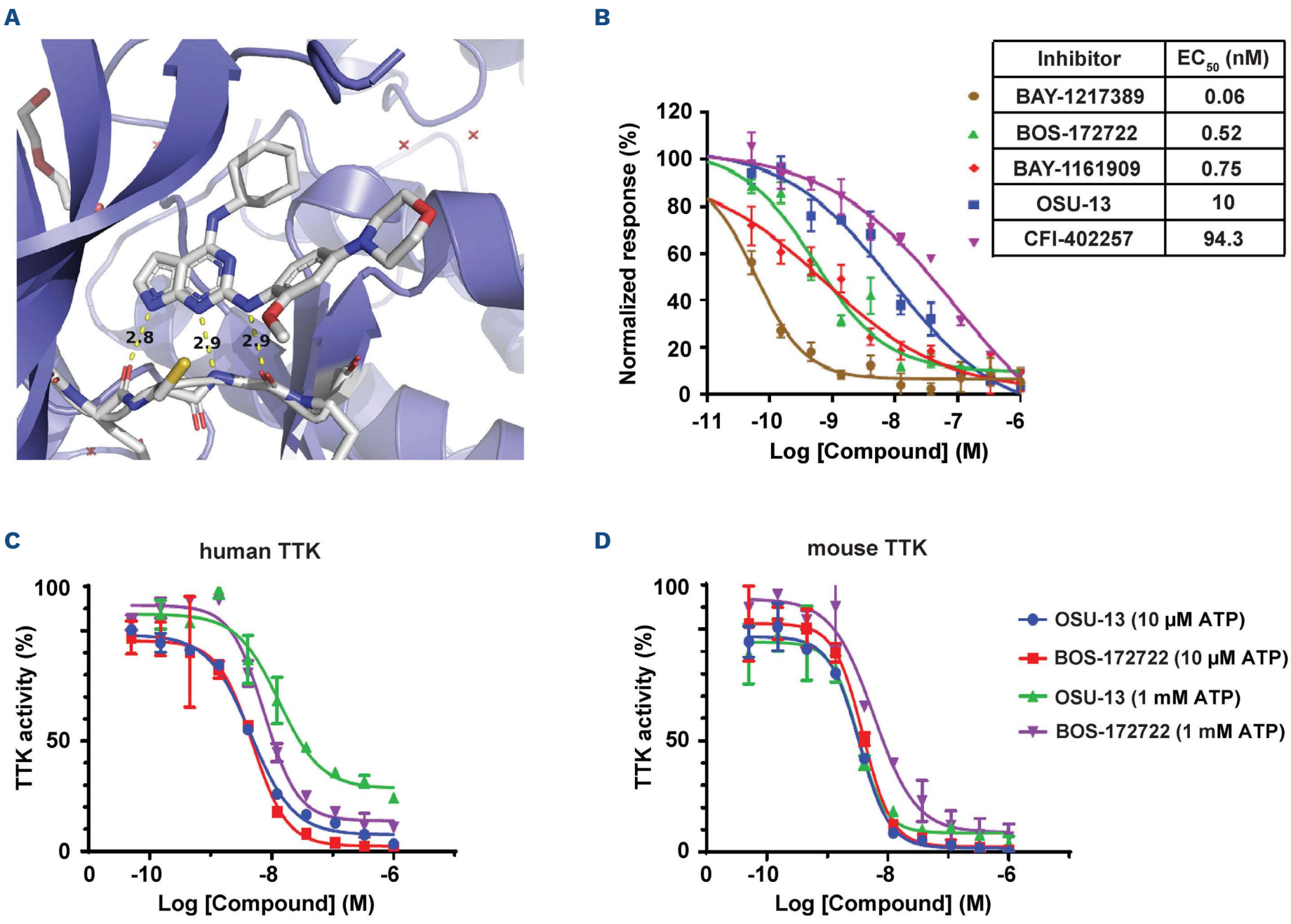

Figure 2 OSU-13 interacts with TTK via hydrogen bonds and inhibits it in low doses and different ATP concentrations. (A) Co-crystal structure of the small molecule inhibitor OSU-13 interacting with TTK. The hydrogen bonds that anchor the adenine binding pocket of OSU-13 to the TTK ATP-binding region are represented by yellow dotted lines. Resolution =2.37 Å, R cryst =20.2, R free =23.3. (B) TTK target engagement assay (NanoBRET™) in HEK293 cells. Relative levels of OSU-13-mediated inhibition of TTK-NanoLuc binding to a fluorescent tracer was measured in comparison to other TTK inhibitors and the half maximal effective concentration (EC_{50}) (nM) was calculated. Graph represents the mean of 2 independent experiments ± standard deviation. (C, D) ADP-Glo kinase assay comparing OSU-13 and BOS-172722 activities at physiologic (1 mM) and low (10 µM) ATP concentrations against the human and mouse TTK enzymes. Inhibition reaction was performed at room temperature for 30 minutes. The graphs show the mean of 2 independent experiments ± standard deviation.

inhibition of TTK-NanoLuc binding to a fluorescent tracer with other reported TTK inhibitors. OSU-13 showed inhibition within the same concentration range as other compounds, with a half maximal effective concentration (EC_{50}) =10 nM, nearly 10-fold lower than the clinical candidate CFI-402257 (EC_{50}=94.3 nM) (Figure 2B). We also verified that OSU-13 inhibits both mouse and human TTK at physiologic (1 mM) and low (10 μM) ATP concentrations, demonstrating activity comparable to the clinical candidate BOS-172722 (Figure 2C, D). Additionally, OSU-13 showed high stability, with a half-life exceeding 90 minutes in human hepatocyte stability assays.

In order to evaluate its selectivity, OSU-13 was profiled against a panel of human kinases in a cell-free kinase activity inhibition assay (*Online Supplementary Table S1*). Among the 399 kinases tested, only seven showed >80% inhibition when incubated with 1 μM OSU-13. Of these, only LRRK2 exhibited a half maximal inhibitory concentration (IC_{50}) in a similar concentration range to TTK/MPS1 (7.5 nM *vs*. 4.3 nM), whereas the other kinases (ALK, IR, LTK, INSRR, and FAK) had IC_{50} values at least 36-fold higher than TTK/MPS1 (Table 1). Importantly, OSU-13 did not significantly inhibit other mitosis-related kinases, such as Aurora kinase, PLK, or Cyclin-dependent kinase family members.

Overall, these results indicate that OSU-13 is a biologically stable molecule that selectively and efficiently inhibits TTK kinase activity, comparable to other TTK/MPS1 inhibitor clinical candidates.

Table 1. OSU-13 inhibitor IC_{50} against select kinases.*

Kinase	OSU-13 IC_{50} (nM)
TTK/MPS1	4.3
LRRK2	7.5
ALK	156.0
IR	262.0
TYK1/LTK	313.0
INSRR	424.0
FAK/PTK2	1009.0

*OSU-13 half maximal inhibitory concentration (IC_{50}) was calculated against the kinases previously inhibited ≥80% at 1 μM OSU-13 during the profiling test (*Online Supplementary Table S1*). Values represent the average of 2 independent experiments.

Table 2. Cytotoxic effect of OSU-13 against human multiple myeloma cell lines with different 1q21 copy numbers.*

Cell line	OSU-13 IC_{50} (nM)	1q21 copy number
EJM	5,870±1,125	3
U266	7,636±791	3
MM.1S	1,106±188	3
RPMI-8226	10,448±1184	4
NCI-H929	867±52	4
JJN3	1,051±127	4
L363	132±1	5
OPM-2	643±109	7
KMS11	309±18	8

*OSU-13 half maximal inhibitory concentration (IC_{50}) values for each cell line represent the mean ± standard deviation from 3 independent MTS assay experiments. Each experiment was performed in triplicate or quadruplicate, and the mean of the replicates was used to generate the curve and calculate the IC_{50}. The 1q21 copy numbers were previously determined by fluorescense *in situ* hybridization.[51]

OSU-13 selectively decreases proliferation and viability of multiple myeloma cells

We investigated the effects of OSU-13 on primary cells derived from the bone marrow of a MM patient and the peripheral blood mononuclear cells (PBMC) of a plasma cell leukemia (PCL) patient. Compared to DMSO, OSU-13 treatment for 72 h reduced viable $CD138^+$ plasma cells from MM and PCL patients by 44% and 18%, respectively (Figure 3A). Only a small effect was observed in viable B cells (reduced by 37% in MM and 6% in PCL) and natural killer (NK) cells (reduced by 11% in MM and 1% in PCL). No significant effect was observed in other lymphocyte populations (*Online Supplementary Figure S3A*). Similarly, PBMC from three healthy donors showed only a 22% decrease in viable B cells in one of the three donors after OSU-13 treatment (*Online Supplementary Figure S3B*). These findings suggest that OSU-13 displays relative selectivity for plasma cells, with mild effects on B-cell lineage lymphocytes and no substantial adverse effects on other PBMC populations.

In order to study OSU-13's effects on human MM cell lines, we evaluated proliferation and viability. Cells were treated with various concentrations of OSU-13 or DMSO, and cell division was monitored using a dye dilution experiment (Figure 3B). OSU-13 decreased proliferation of OPM-2 and NCI-H929 cell lines in a dose-dependent manner. At 5 μM OSU-13, proliferation decreased to 54±10% and 49±4% compared to DMSO control in OPM-2 and NCI-H929, respectively (P<0.01). RPMI-8226 and U266 showed a less pronounced effect on proliferation (*data not shown*).

The cytotoxic potential of OSU-13 was evaluated via MTS assay in nine human MM cell lines with different 1q21 copy numbers (Table 2). L363 was the most sensitive (IC_{50}=132±1 nM) cell line, whereas RPMI-8226 was the least sensitive (IC_{50}=10,448±1,184 nM) to OSU-13. Further analysis revealed a significant inverse correlation (rs=-0.76; P=0.017) between the number of 1q21 copies and the *in vitro* IC_{50} of OSU-13. MM cell lines with a higher number of 1q21 copies exhibited increased sensitivity to OSU-13. This finding suggests that OSU-13, through TTK inhibition, is particularly effective in a subgroup of high-risk MM patients with a poor prognosis.

Next, we assessed viability of NCI-H929 and OPM-2 cells using Zombie staining (Figure 3C). DMSO-treated cells

showed an increase in viable cell numbers over time, while OSU-13-treated cells remained constant. After 72 h, the quantity of viable DMSO-treated cells was 5-fold and 3.6-fold higher (P<0.05) than OSU-13-treated cells in OPM-2 and NCI-H929, respectively (Figure 3C, left). The percentage of dead cells (Zombie$^+$) peaked after 72 h, reaching 35±4.5% of OPM-2 (P<0.01) and 21±6.3% of NCI-H929 cells (P<0.05). Meanwhile, DMSO-treated cells did not show increase in Zombie$^+$ cells over time (Figure 3C, right). Moreover, some dead cells turned into debris, resulting in a smaller Zombie$^+$ population than expected.

OSU-13 induces apoptosis in human multiple myeloma cell lines through caspase activation

In order to investigate whether OSU-13-induced cell death was apoptotic, caspase 3 and 7 activity was assessed in NCI-H929 cells at different time points after treatment with varying concentrations of OSU-13. Caspase 3 and 7

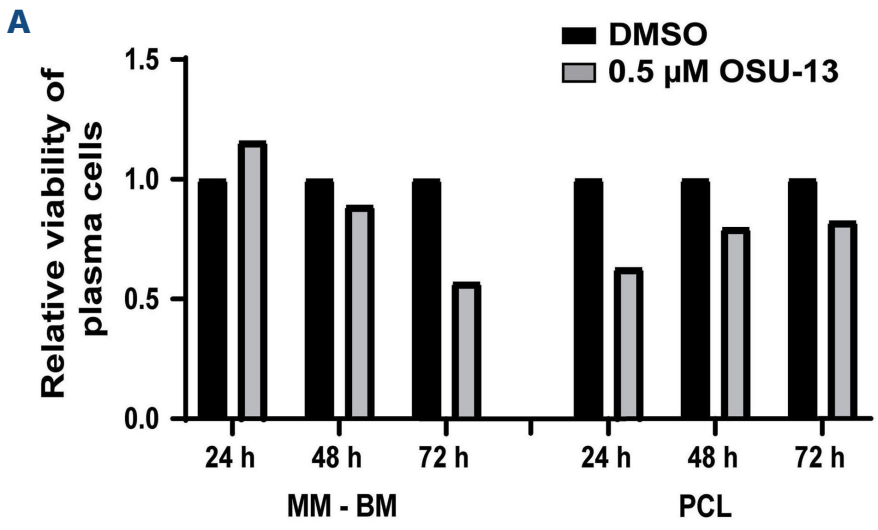

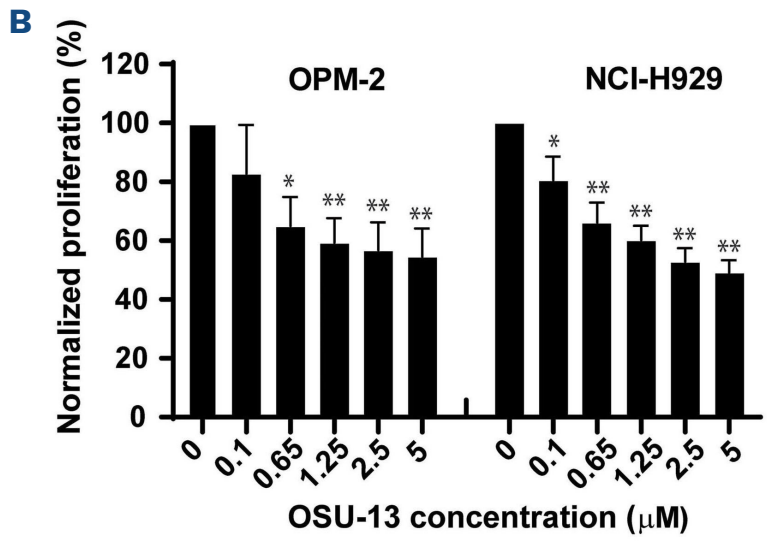

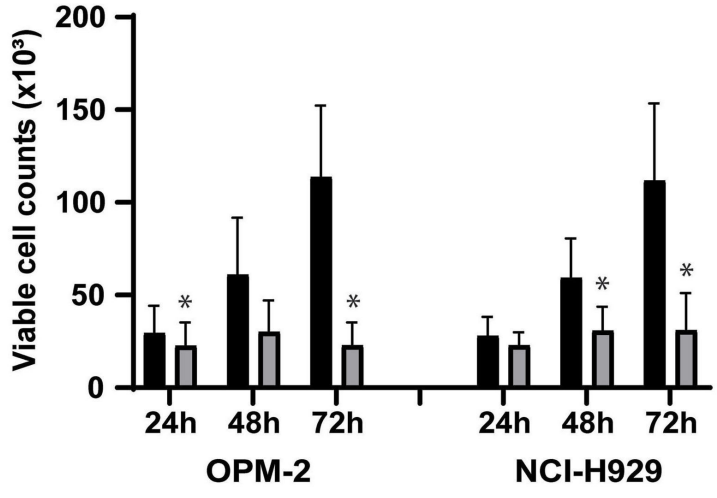

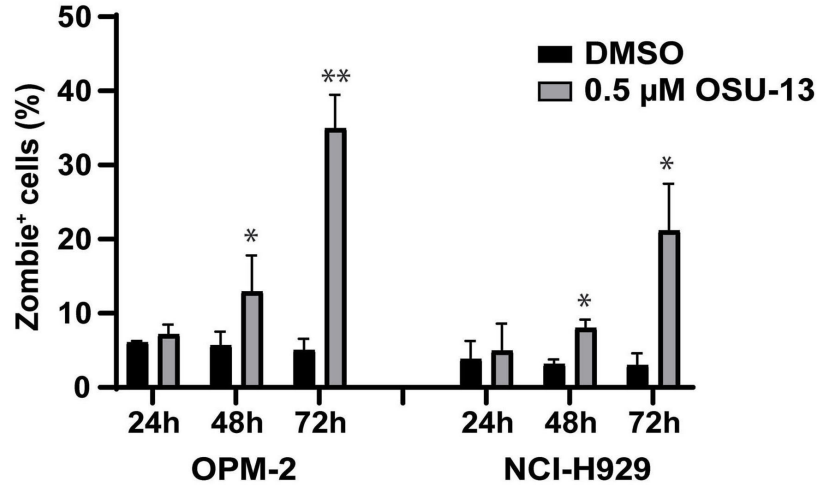

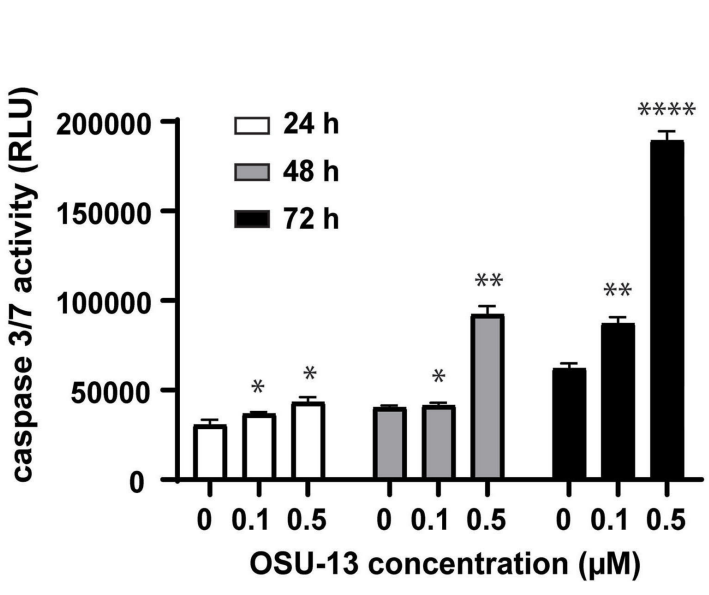

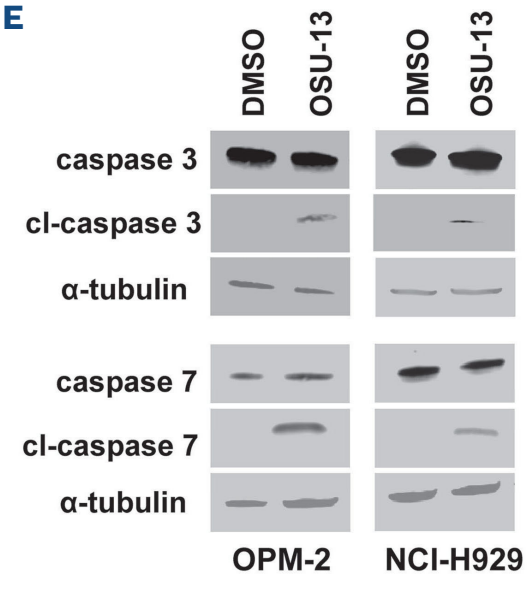

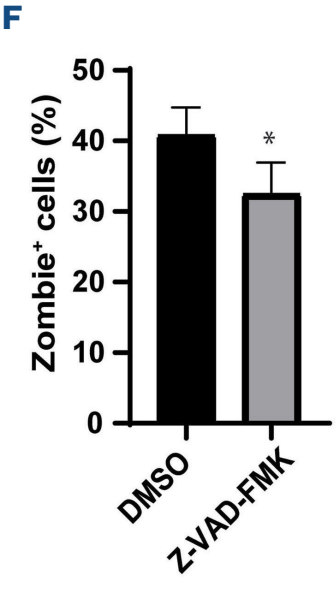

Continued on following page.

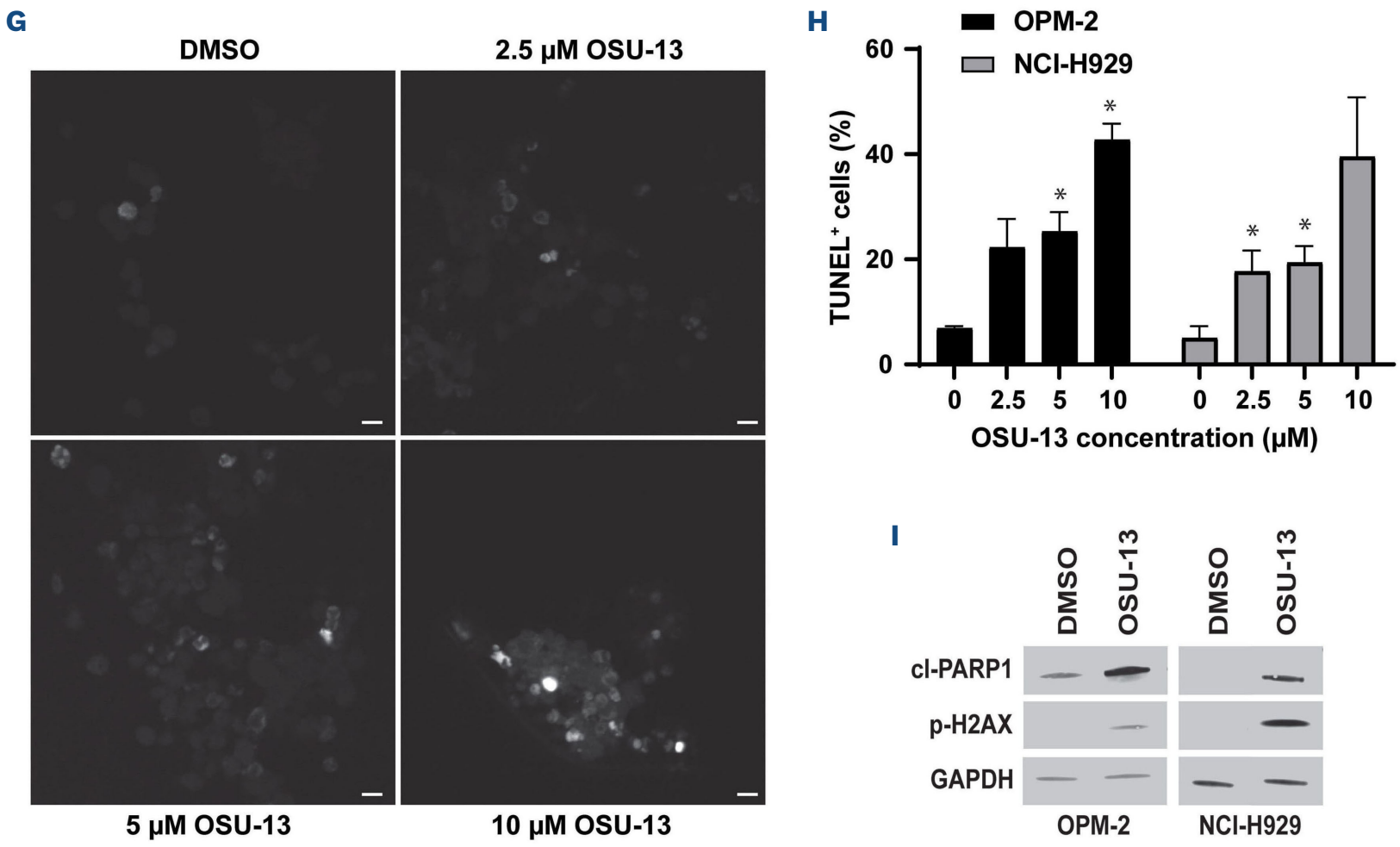

Figure 3. OSU-13 decreases viability, induces apoptosis, and causes DNA damage in human multiple myeloma cells. (A) Primary cells derived from the bone marrow of a multiple myeloma (MM) patient and the peripheral blood mononuclear cells of a plasma cell leukemia (PCL) patient were cultured *in vitro* at 37°C in dimethyl sulfoxide (DMSO) ±0.5 µM of OSU-13 for 24, 48, and 72 hours (h). The graph shows the comparative viability of $CD138^+$ plasma cells ($Zombie^-$) treated with OSU-13 relative to DMSO. (B) Relative proliferation of OPM-2 (left) and NCI-H929 (right) MM cell lines after incubation with 0, 0.1, 0.65, 1.25, 2.5, and 5 µM of OSU-13 for 72 h. The average of DMSO control data (concentration 0) was set to 100%. Proliferation was calculated using Cell Trace Far Red. Data shown are the mean of 3 independent experiments ± standard deviation (SD); $^*P$<0.05; $^{**}P$<0.01 in relation to DMSO. (C) OPM-2 (left) and NCI-H929 (right) cells were incubated in DMSO or 0.5 µM OSU-13 for 24, 48, and 72 h, and assessed for viability through Zombie staining. Viable cell counts ($Zombie^-$; left panel) and percentage of dead cells ($Zombie^+$; right panel) were analyzed by flow cytometry. Data represent the mean of 3 independent experiments ± SD; $^*P$<0.05; $^{**}P$<0.01. (D) Activity of caspases 3 and 7 in NCI-H929 after 24, 48, and 72 h treatment with 0, 0.1, and 0.5 µM OSU-13 assessed by ApoTox-Glo™Triplex assay. Data represent the mean ± SD (N=3); $^*P$<0.05; $^{**}P$<0.01; $^{****}P$<0.0001. (E) Western blot analysis of caspase 3, cleaved caspase 3, caspase 7, and cleaved caspase 7 in lysates from OPM-2 (left) and NCI-H929 (right) cells incubated in DMSO or 0.5 µM OSU-13 for 72 h. α-tubulin was used as loading control. Images depict a representative experiment from 3 independent biological replicates. (F) Effect of Z-VAD-FMK in OSU-13-induced apoptosis. OPM-2 cells were pre-incubated for 1 h with 100 µM Z-VAD-FMK or DMSO, washed with phosphate-buffered saline, and incubated for 72 h in 1 µM OSU-13. Cell viability was assessed with Zombie-aqua dye staining by flow cytometry. Data represent the mean of 3 independent experiments ± SD; $^*P$<0.05. (G) TUNEL staining analysis of OPM-2 and NCI-H929 cells treated with DMSO or OSU-13 (2.5, 5, and 10 µM) for 48 h. Representative fluorescence microscopy images from a spinning-disk confocal system (UltraVIEW) on a Nikon Ti-E microscope show $TUNEL^+$ staining indicating DNA damage in OPM-2 cells. Scale bars, 20 µm. (H) TUNEL images were manually quantified in ImageJ and TUNEL positivity rate (%) was calculated. Results are representative of 2 independent experiments for each cell line; $^*P$<0.05. (I) Western blot analysis of cleaved PARP1 and p-H2AX in lysates from OPM-2 and NCI-H929 cells incubated in DMSO or 0.5 µM OSU-13 for 72 h. GAPDH was used as loading control. Images depict a representative experiment from 4 independent experiments. RLU: relative luminescence unit.

activation started at 24 h with 0.1 µM (P<0.05) and peaked after 72 h with 0.5 µM OSU-13 (P<0.0001) (Figure 3D). Accordingly, western blot analysis of cell lysates showed increased levels of cleaved caspases 3 and 7 in OPM-2 and NCI-H929 cells after 72 h of OSU-13 treatment (Figure 3E), and pretreatment with the pan-caspase inhibitor Z-VAD-FMK decreased OSU-13-mediated cell death by 20±6.7% in OPM-2 cells (Figure 3F). In contrast, pretreatment with the necroptosis inhibitor Necrostatin-1s had no measurable effect on cell death, and there was no increase in the autophagy marker LC3B following OSU-13 treatment (*Online Supplementary Figure S4A, B,* respectively). Collectively, these results indicate that OSU-13 triggers cell death in MM cell lines through caspase activation, and that apoptosis - but not necroptosis or autophagy - is partially responsible for this OSU-13-mediated cell death.

OSU-13 induces DNA damage in multiple myeloma cell lines

Apoptosis has been reported to induce DNA fragmentation. In order to measure internucleosomal DNA degradation, we treated OPM-2 and NCI-H929 cells with various concen-

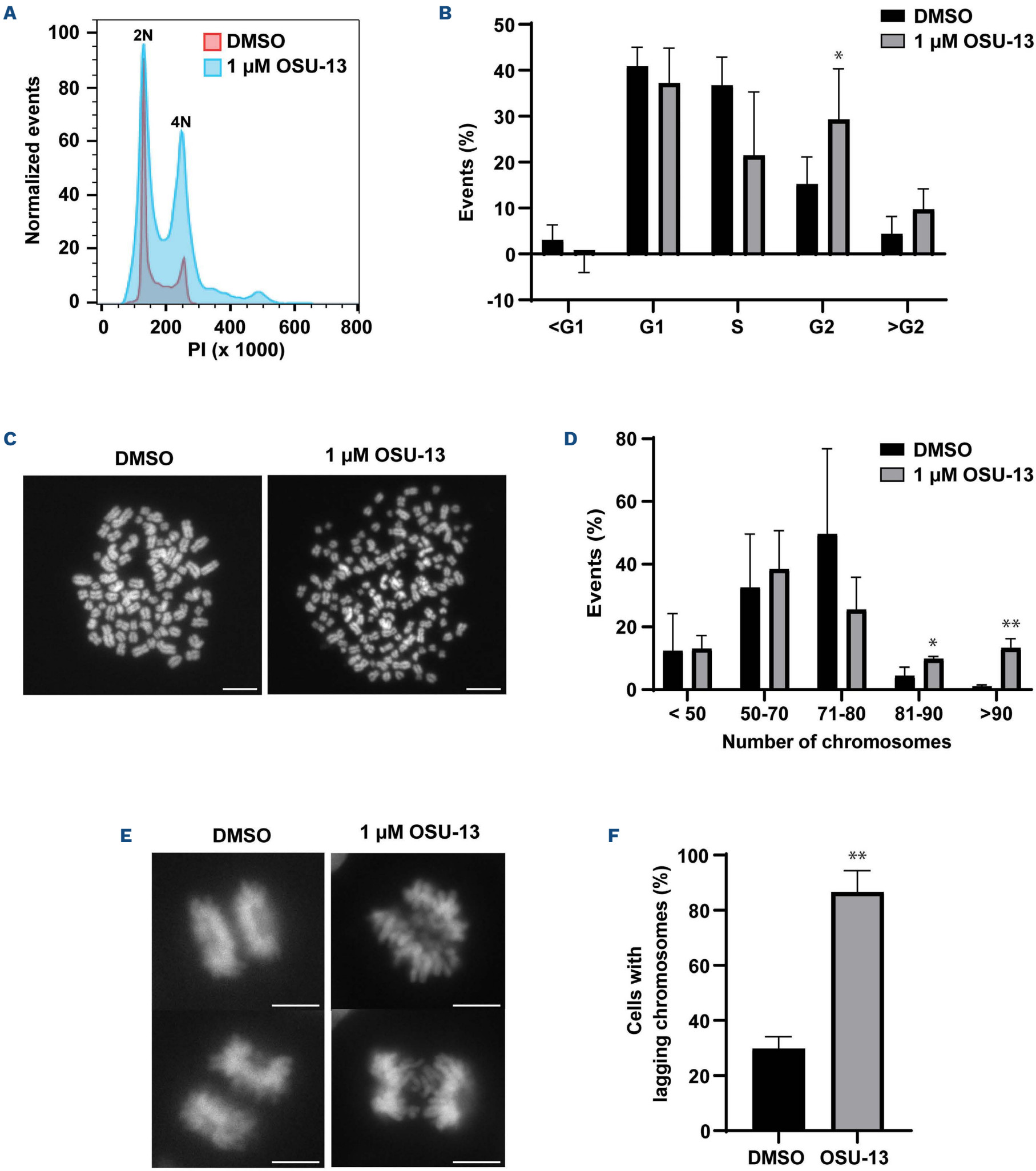

Figure 4. OSU-13 causes cell cycle and chromosome segregation abnormalities in OPM-2 cells. (A) DNA content analysis of OPM-2 cells treated with dimethyl sulfoxide (DMSO) (red) or 1 µM OSU-13 (blue) for 72 hours (h). After treatment, DNA was stained with the intercalating agent propidium iodide (PI) and analyzed by flow cytometry. 2N and 4N populations are indicated. Data are representative of 4 independent experiments. (B) Graphical representation of the cell cycle analysis from data depicted in panel (A). Analysis was performed by the Cell Cycle tool in FlowJo_V10 software using the Watson model. Results are mean ± standard deviation of 4 independent experimental replicates; $^{*}P<0.05$. (C, D) Chromosome spread analysis of OPM-2 cells treated with

Continued on following page.

DMSO or 1 μM OSU-13 for 24 h. Slides were mounted in Prolong Glass Antifade Mountant with NucBlue to stain the chromosomes and imaged in a Nikon DM5000 B microscope. (C) representative fluorescence microscopy images depict metaphase spreads. Scale bars, 10 μm. (D) graph shows distribution of the cell population according to the number of chromosomes, manually quantified in ImageJ. Results are representative of 3 independent experiments; $^{*}P<0.05$; $^{**}P<0.01$. (E, F) Analysis of chromosome segregation during metaphase/anaphase. OPM-2 cells were synchronized by double thymidine block, released, and treated (1 μM OSU-13 or DMSO) for 9 h. Samples were mounted with NucBlue to stain the chromosomes. (E) representative fluorescence images from cells during chromosome alignment and segregation. Scale bars, 10 μm. (F) graph shows the mean percentage of cells with lagging chromosomes ± standard deviation from 2 independent experiments; $^{**}P<0.01$.

trations of OSU-13 for 48 h and performed TUNEL analysis. DNA damage increased in a dose-dependent manner in both cell lines, as indicated by the correlation between OSU-13 concentration and percentage of TUNEL^{+} cells (Figure 3G, H). In OPM-2 cells, TUNEL positivity rates were 22±5.4%, 25±3.6% ($P<0.05$), and 43±3.1% ($P<0.05$) with 2.5 μM, 5 μM, and 10 μM OSU-13 treatment, respectively, compared to DMSO control (TUNEL^{+} =7±0.4%). In NCI-H929, TUNEL positivity increased with 2.5 μM OSU-13 treatment ($P<0.05$) (Figure 3H). Western blot analysis confirmed the presence of DNA damage, showing increased levels of p-H2AX and cleaved PARP1 after 72 hours of OSU-13 treatment (Figure 3I).

OSU-13 interferes in the cell cycle and ploidy of multiple myeloma cell lines

TTK/MPS1 inhibitors affect the cell cycle in a variety of cancer cells.[30,33,35] In our study, treatment with OSU-13 induced significant alterations in DNA content in OPM-2 cells, with an increase in tetraploid (4N) and hyperploid (>4N) cells (Figure 4A). Accordingly, flow cytometric analysis revealed a substantial increase in the proportion of OPM-2 cells in the G2 phase (4N) after OSU-13 treatment, with a 1.9-fold increase compared to DMSO-treated cells ($P<0.05$). Additionally, there was a higher proportion of cells in the >G2 phase (>4N), although this difference was not statistically significant (Figure 4B).

This increase in the hyperploid population was confirmed by fluorescence microscopy of OPM-2 chromosome spreads (Figure 4C, D). There was a higher quantity of chromosomes (Figure 4C), with a significant increase in cells with more than 91 chromosomes (13.2±2.9% in OSU-13 *vs.* 0.9±0.5% in DMSO; $P<0.01$). In addition, cells with 81-90 chromosomes also increased (9.7±0.8% in OSU-13 *vs.* 4.4±2.7% in DMSO; $P<0.05$) (Figure 4D). Similar effects were observed in NCI-H929 cells (*Online Supplementary Figure S5A-C*).

Chromosome segregation was analyzed by microscopy to understand the mechanism behind this increase in the hyperploid population. OPM-2 cells treated with OSU-13 exhibited severe defects in chromosome alignment and segregation (Figure 4E), with 86.6±7.7% of the cells ($P<0.01$) presenting lagging chromosomes during anaphase (Figure 4F).

OSU-13 has *in vivo* effect against multiple myeloma in mice

The therapeutic potential of OSU-13 was evaluated in an NCI-H929 subcutaneous MM xenograft model in immunodeficient CB.17 SCID mice (Figure 5). Mice were treated daily per oral gavage starting 14 days after tumor implantation (day -14). Vehicle control or 10 mg/kg dose of OSU-13 were administered for 21 days, with a dosing holiday on days 14-17 due to unexpected weight loss in the OSU-13-treated group (Figure 5A). Treatment with OSU-13 produced a significant delay in tumor growth (Figure 5B). On average, vehicle-treated mice reached the endpoint tumor volume (≥2,000 mm^3) by day 18, whereas OSU-13-treated mice only achieved this size on day 25. At day 18, 50% of vehicle-treated mice reached the threshold, compared to only 10% of OSU-13-treated mice ($P<0.05$). In addition, the average tumor volume in the OSU-13-treated group was half of the vehicle-treated group (1,084 mm^3 *vs.* 1,980 mm^3). Treatment ended on day 21, justifying the increased tumor growth after this date. Altogether, treatment with OSU-13 resulted in a 22% tumor growth delay ($P<0.05$) and showed superior efficacy compared to the clinical candidate CFI-402257 in a parallel experiment (*data not shown*).

In another MM xenograft model using NOD SCID mice (Figure 5C), OSU-13 treatment also led to a significant delay in tumor growth. By the end of the treatment period (day 14), the average tumor volume in the OSU-13-treated group was 453 mm^3, significantly lower than the control group (681 mm^3; $P<0.05$) (Figure 5D). In addition, western blot analysis of tumor lysates showed increased expression of the apoptosis markers cleaved-caspase 3 and p-H2AX in the OSU-13-treated group (Figure 5E, F). These findings demonstrate that OSU-13 effectively reduces MM tumor burden and induces apoptosis in MM cells *in vivo*.

Discussion

TTK/Mps1 plays an essential role in SAC,[24] and high levels of *TTK* expression correlate to unfavorable prognosis in several cancers.[25-28,34] Accordingly, TTK inhibition has been explored in solid tumors as a therapeutic strategy to halt cell cycle arrest and induce genomic instability.[28,30-33] However, the impact of *TTK* expression and TTK/MPS1 inhibition in hematologic cancers remains poorly understood.[36,37]

Here, we show that elevated *TTK* expression correlates with reduced overall and event-free survival along with amplification or gain of 1q21, found in high-risk MM. Indeed, *TTK* expression is significantly increased in high-risk compared to low-risk MM,[36] and TTK is included in the MM Kinome

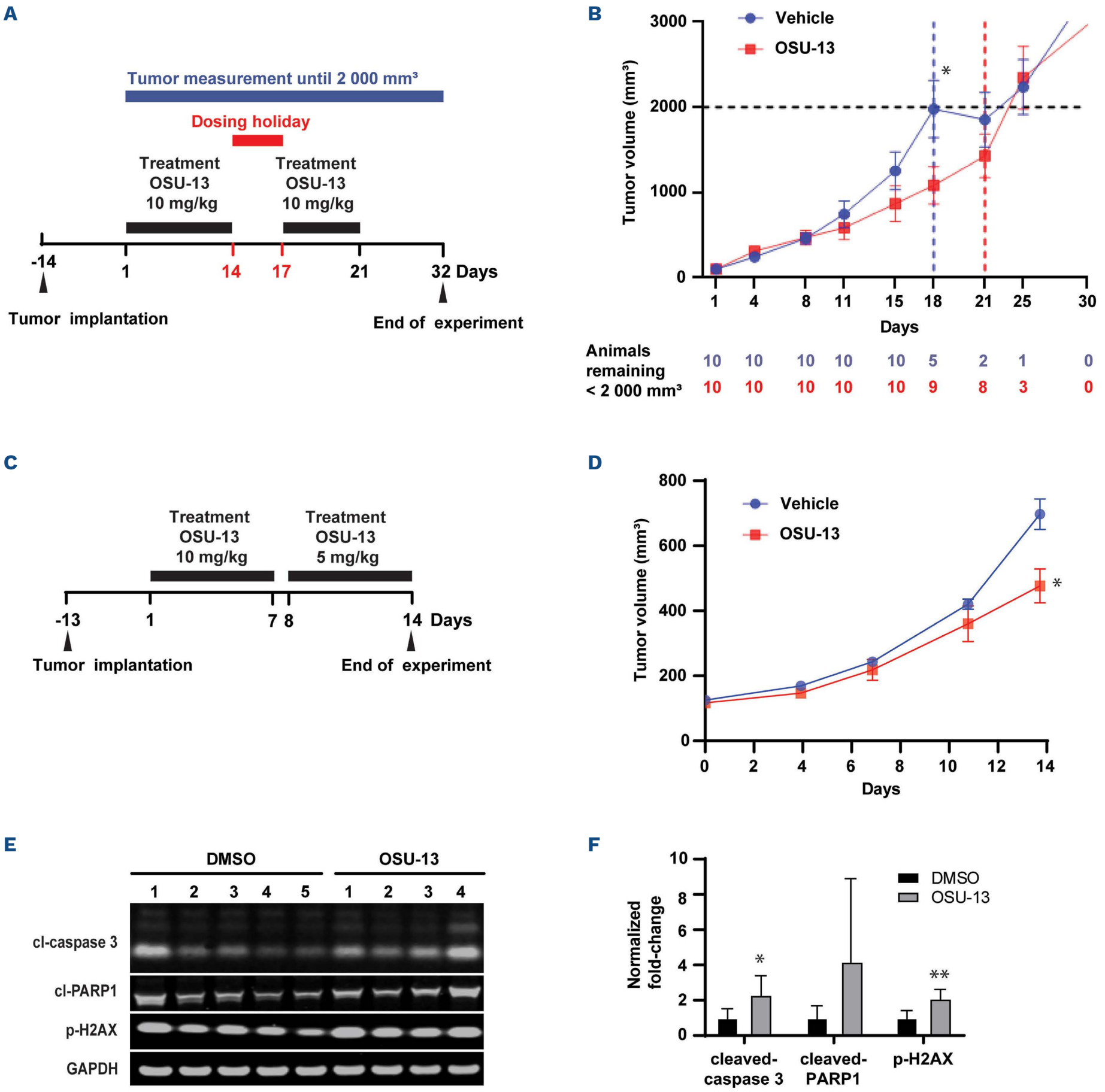

Figure 5 OSU-13 shows therapeutic potential in mouse model. (A, B) Human multiple myeloma (MM) NCI-H929 cells were subcutaneously inoculated in immunodeficient CB.17 SCID mice. Fourteen days post-implantation, mice were treated orally daily with the vehicle control or 10 mg/kg of OSU-13 for 21 days, with a dosing holiday from days 14-17 due to weight loss. (B) Graphical representation of the mean ± standard error the mean tumor volume of the vehicle- (blue) and OSU-13-treated (red) groups over time (N=10 mice per group). The black dashed line indicates the 2,000 mm^3 tumor volume threshold, the blue dashed line highlights the 18th day of experiment, and the red dashed line stresses the day when treatment was stopped; $^*P<0.05$. The number of animals remaining in the study (tumor volume <2,000 mm^3) are indicated for the vehicle- (blue) and OSU-13-treated (red) groups. (C) NCI-H929 cells were subcutaneously injected into immunodeficient NOD SCID mice. Thirteen days after implantation, the mice were subjected to daily oral treatment with either the vehicle control or OSU-13 (10 mg/kg on days 1-7 and 5 mg/kg on days 8-14). After 24 hours of treatment, the mice were euthanized, and the tumors were collected for further analysis. (D) Graphical representation of the mean ± standard error the mean tumor volume of the vehicle- (blue) and OSU-13-treated (red) groups over time (N=5 mice per group); $^*P<0.05$. (E) Western blot analysis of tumor lysates from the experiment described in (C). Expression of cleaved caspase 3, cleaved PARP1 and p-H2AX are shown with GAPDH as a loading control. Individual results from each mouse are shown in the images. (F) Quantification of the western blot analysis depicted in panel (E). Results are mean ± standard deviation; $^*P<0.05$; $^{**}P<0.01$.

Index, a gene expression profile risk score that predicts poor prognosis in MM.[36]

We report the first comprehensive analysis of a TTK/MPS1 inhibitor, OSU-13, in MM. Co-crystal structures reveal its binding to the ATP-binding pocket of TTK similarly to other TTK/MPS1 inhibitors,[33,38] suggesting a conserved mechanism of inhibition. OSU-13 is stable and selectively inhibits TTK, showing comparable activity to the TTK/MPS1 inhibitor clinical candidates CFI-402257 and BOS-172722, which reinforces its clinical potential.

OSU-13 exhibited similar effects in MM as previously observed in breast cancer[31] or with other TTK inhibitors in several cancers.[29,30,32,33]

First, OSU-13 showed cytotoxicity and anti-proliferative activity across MM cell lines. Sensitivity to OSU-13 varied among cell lines and correlated with 1q21 copy number. Nonetheless, sensitivity to TTK/MPS1 inhibitors seems to be multifactorial as observed in other cancer types,[29,35] and identifying additional predictive biomarkers would further define patients who might benefit from TTK/MPS1 inhibitor-based therapies, expanding the potential applications of these treatments.

Second, OSU-13 induced apoptosis in MM cells, evidenced by caspase 3 and 7 activation and DNA damage, indicated by PARP1 cleavage, phosphorylation of H2AX, and TUNEL assay. However, partial rescue by the caspase inhibitor Z-VAD-FMK suggested involvement of caspase-independent mechanisms in OSU-13-induced cell death. Unlike the TTK/MPS1 inhibitor reversine that triggers autophagy by increasing LC3-B and Beclin 1 via the AKT pathway in cholangiocarcinoma cells,[39] it seems that OSU-13 does not induce autophagy or necroptosis in MM cell lines.

Third, OSU-13 triggered abnormal mitosis, leading to chromosome missegregation, aneuploidy, and elevated chromosome numbers. Comparable effects have been reported in hematologic cancers with the TTK/MPS1 inhibitor AZ3146, inducing chromosome instability and DNA damage in MM[36] and acute myeloid leukemia.[37]

Lastly, OSU-13 achieved significant tumor growth delay in NCI-H929 xenografts in two immunodeficient mouse models, despite a 3-day treatment interruption and a dose reduction due to weight loss. In a breast cancer mouse model, OSU-13 previously reduced tumor growth without affecting body weight.[31] However, the aforementioned study used athymic nude mice, potentially less sensitive to OSU-13 than the CB.17 SCID and NOD SCID mice we used.

OSU-13 showed modest efficacy in our experiment as a single agent. Combination strategies for TTK/MPS1 inhibitors have been explored in various cancer models. Combination with the anti-programmed cell death 1 (PD-1) antibody was more effective than monotherapy in a colon cancer model.[35] TTK inhibition also sensitized cells to paclitaxel treatment in colon,[33] breast, and lung cancers.[32] Accordingly, clinical trials with CFI-402257 are currently investigating combination therapies with paclitaxel and fulvestrant for breast cancer treatment. Standard-of-care therapies for MM involve combinations of different agents to enhance response and prevent resistance. However, the combination strategies used for TTK inhibitors in solid tumors are unlikely to succeed in MM. Clinical trials with PD-1/PD-L1 inhibitors have shown limited results in MM - probably due to the immunosuppressive environment in MM - and have been halted due to severe adverse effects.[40] Similarly, studies with the albumin-bound formulation Nab-paclitaxel[41] did not achieve sustained responses in MM.[42]

In acute myeloid leukemia, the TTK inhibitor AZ3146 induced robust upregulation of the interferon gene,[37] which has both direct anti-cancer effects[43,44] and immune-activation potential.[45-47] It would be interesting to investigate whether TTK inhibition triggers similar immunological effects in MM, potentially enhancing the effect of immunomodulatory drugs. In addition, MM cells may be sensitized to TTK inhibition by DNA-damaging agents such as proteasome inhibitors, alkylating agents, or experimental drugs that induce DNA double-strand breaks.[48-50] Indeed, our initial findings suggest synergistic effects of OSU-13 with melphalan, a DNA-damaging agent. Identifying optimal combination strategies for OSU-13 will provide maximum efficacy and tolerability in MM treatment, providing new treatment options for relapsed/refractory MM patients.

In summary, our findings emphasize the importance of TTK in MM prognosis and show that OSU-13-mediated TTK inhibition induces cell death in MM cell lines and reduces tumor growth *in vivo*. We propose that inhibition of TTK using OSU-13 is an effective approach for treating multiple myeloma, particularly in a significant subgroup of high-risk patients with poor prognosis. Importantly, this is the first time that TTK inhibition has been comprehensively explored as a potential therapeutic strategy for a hematologic malignancy.

Disclosures

No conflicts of interest to disclose.

Contributions

LVGL, BM-L, FC, TH and GH conceptualized and designed experiments, validated and analyzed data. LVGL, BM-L, TH and FC performed experiments. LVGL, TH and FC designed and created figures for the manuscript. LVGL wrote the manuscript, and FC, TH, GH and EM reviewed and edited the manuscript. DB advised on experimental design and data analysis, supervised, and provided resources for the study.

Acknowledgments

The authors would like to thank the OSU Comprehensive Cancer Center Leukemia Tissue Bank, the OSUCCC support (core) grant (CCSG) 2P30CA016058-45, Dr. Jian-Qiu Wu and the OSU Molecular Genetics Department for the use of the fluorescence and confocal microscopes, and the OSU

Comprehensive Cancer Center Drug Development Institute for providing the OSU-13 drug and collaborating with experiments and discussions.

Funding

This work was supported by OSU divisional funds (to DB and FC), the Pelotonia Foundation (to FC and BM), the Paula and Rodger Riney Foundation (to DB and FC), the Elsa U. Pardee Foundation (to FC), the International Myeloma Society (to FC), the National Cancer Institute (1K08CA263476-01A1 to FC) and the OSU Comprehensive Cancer Center Drug Development Institute.

Data-sharing statement

The data are available from the corresponding author upon request.

References

1. Siegel RL, Miller KD, Jemal A. Cancer statistics, 2019. CA Cancer J Clin. 2019;69(1):7-34.
2. Attal M, Lauwers-Cances V, Hulin C, et al. Lenalidomide, bortezomib, and dexamethasone with transplantation for myeloma. N Engl J Med. 2017;376(14):1311-1320.
3. Mikkilineni L, Kochenderfer JN. Chimeric antigen receptor T-cell therapies for multiple myeloma. Blood. 2017;130(24):2594-2602.
4. Robak P, Drozdz I, Szemraj J, Robak T. Drug resistance in multiple myeloma. Cancer Treat Rev. 2018;70:199-208.
5. Bharadwaj R, Yu H. The spindle checkpoint, aneuploidy, and cancer. Oncogene. 2004;23(11):2016-2027.
6. Kops GJ, Weaver BA, Cleveland DW. On the road to cancer: aneuploidy and the mitotic checkpoint. Nat Rev Cancer. 2005;5(10):773-785.
7. Neuse CJ, Lomas OC, Schliemann C, et al. Genome instability in multiple myeloma. Leukemia. 2020;34(11):2887-2897.
8. Drach J, Schuster J, Nowotny H, et al. Multiple-myeloma - high-incidence of chromosomal aneuploidy as detected by interphase fluorescence in-situ hybridization. Cancer Res. 1995;55(17):3854-3859.
9. Bergsagel PL, Kuehl WM. Chromosome translocations in multiple myeloma. Oncogene. 2001;20(40):5611-5622.
10. Bergsagel PL, Kuehl WM. Molecular pathogenesis and a consequent classification of multiple myeloma. J Clin Oncol. 2005;23(26):6333-6338.
11. Sawyer JR. The prognostic significance of cytogenetics and molecular profiling in multiple myeloma. Cancer Genet. 2011;204(1):3-12.
12. Shammas MA, Shmookler Reis RJ, Koley H, Batchu RB, Li C, Munshi NC. Dysfunctional homologous recombination mediates genomic instability and progression in myeloma. Blood. 2009;113(10):2290-2297.
13. Chng WJ, Fonseca R. Centrosomes and myeloma; aneuploidy and proliferation. Environ Mol Mutagen. 2009;50(8):697-707.
14. Lara-Gonzalez P, Westhorpe FG, Taylor SS. The spindle assembly checkpoint. Curr Biol. 2012;22(22):R966-980.
15. Musacchio A, Salmon ED. The spindle-assembly checkpoint in space and time. Nat Rev Mol Cell Biol. 2007;8(5):379-393.
16. Thompson SL, Bakhoum SF, Compton DA. Mechanisms of chromosomal instability. Curr Biol. 2010;20(6):R285-295.
17. Diaz-Rodriguez E, Sotillo R, Schvartzman JM, Benezra R. Hec1 overexpression hyperactivates the mitotic checkpoint and induces tumor formation in vivo. Proc Natl Acad Sci U S A. 2008;105(43):16719-16724.
18. Sotillo R, Hernando E, Diaz-Rodriguez E, et al. Mad2 overexpression promotes aneuploidy and tumorigenesis in mice. Cancer Cell. 2007;11(1):9-23.
19. Borisa AC, Bhatt HG. A comprehensive review on aurora kinase: small molecule inhibitors and clinical trial studies. Eur J Med Chem. 2017;140:1-19.
20. Talati C, Griffiths EA, Wetzler M, Wang ES. Polo-like kinase inhibitors in hematologic malignancies. Crit Rev Oncol Hematol. 2016;98:200-210.
21. Chung V, Heath EI, Schelman WR, et al. First-time-in-human study of GSK923295, a novel antimitotic inhibitor of centromere-associated protein E (CENP-E), in patients with refractory cancer. Cancer Chemother Pharmacol. 2012;69(3):733-741.
22. Wei JH, Chou YF, Ou YH, et al. TTK/hMps1 participates in the regulation of DNA damage checkpoint response by phosphorylating CHK2 on threonine 68. J Biol Chem. 2005;280(9):7748-7757.
23. Fisk HA, Mattison CP, Winey M. Human Mps1 protein kinase is required for centrosome duplication and normal mitotic progression. Proc Natl Acad Sci U S A. 2003;100(25):14875-14880.
24. Liu X, Winey M. The MPS1 family of protein kinases. Annu Rev Biochem. 2012;81:561-585.
25. Slee RB, Grimes BR, Bansal R, et al. Selective inhibition of pancreatic ductal adenocarcinoma cell growth by the mitotic MPS1 kinase inhibitor NMS-P715. Mol Cancer Ther. 2014;13(2):307-315.
26. Zhang L, Jiang B, Zhu N, et al. Mitotic checkpoint kinase Mps1/TTK predicts prognosis of colon cancer patients and regulates tumor proliferation and differentiation via PKCalpha/ERK1/2 and PI3K/Akt pathway. Med Oncol. 2019;37(1):5.
27. Al-Ejeh F, Simpson PT, Saunus JM, et al. Meta-analysis of the global gene expression profile of triple-negative breast cancer identifies genes for the prognostication and treatment of aggressive breast cancer. Oncogenesis. 2014;3:e124.
28. Tannous BA, Kerami M, Van der Stoop PM, et al. Effects of the selective MPS1 inhibitor MPS1-IN-3 on glioblastoma sensitivity to antimitotic drugs. J Natl Cancer Inst. 2013;105(17):1322-1331.
29. Colombo R, Caldarelli M, Mennecozzi M, et al. Targeting the mitotic checkpoint for cancer therapy with NMS-P715, an inhibitor of MPS1 kinase. Cancer Res. 2010;70(24):10255-10264.
30. Tardif KD, Rogers A, Cassiano J, et al. Characterization of the cellular and antitumor effects of MPI-0479605, a small-molecule inhibitor of the mitotic kinase Mps1. Mol Cancer Ther. 2011;10(12):2267-2275.
31. Sugimoto Y, Sawant DB, Fisk HA, et al. Novel pyrrolopyrimidines as Mps1/TTK kinase inhibitors for breast cancer. Bioorg Med Chem. 2017;25(7):2156-2166.
32. Wengner AM, Siemeister G, Koppitz M, et al. Novel Mps1 kinase inhibitors with potent antitumor activity. Mol Cancer Ther. 2016;15(4):583-592.
33. Jemaa M, Galluzzi L, Kepp O, et al. Characterization of novel

MPS1 inhibitors with preclinical anticancer activity. Cell Death Differ. 2013;20(11):1532-1545.
34. Choi M, Min YH, Pyo J, Lee CW, Jang CY, Kim JE. TC Mps1 12, a novel Mps1 inhibitor, suppresses the growth of hepatocellular carcinoma cells via the accumulation of chromosomal instability. Br J Pharmacol. 2017;174(12):1810-1825.
35. Mason JM, Wei X, Fletcher GC, et al. Functional characterization of CFI-402257, a potent and selective Mps1/TTK kinase inhibitor, for the treatment of cancer. Proc Natl Acad Sci U S A. 2017;114(12):3127-3132.
36. de Boussac H, Bruyer A, Jourdan M, et al. Kinome expression profiling to target new therapeutic avenues in multiple myeloma. Haematologica. 2020;105(3):784-795.
37. Jin N, Lera RF, Yan RE, et al. Chromosomal instability upregulates interferon in acute myeloid leukemia. Genes Chromosomes Cancer. 2020;59(11):627-638.
38. Kwiatkowski N, Jelluma N, Filippakopoulos P, et al. Small-molecule kinase inhibitors provide insight into Mps1 cell cycle function. Nat Chem Biol. 2010;6(5):359-368.
39. Prajumwongs P, Waenphimai O, Vaeteewoottacharn K, Wongkham S, Sawanyawisuth K. Reversine, a selective MPS1 inhibitor, induced autophagic cell death via diminished glucose uptake and ATP production in cholangiocarcinoma cells. PeerJ. 2021;9:e10637.
40. Oliva S, Troia R, D'Agostino M, Boccadoro M, Gay F. Promises and pitfalls in the use of PD-1/PD-L1 inhibitors in multiple myeloma. Front Immunol. 2018;9:2749.
41. Desai N, Trieu V, Yao Z, et al. Increased antitumor activity, intratumor paclitaxel concentrations, and endothelial cell transport of cremophor-free, albumin-bound paclitaxel, ABI-007, compared with cremophor-based paclitaxel. Clin Cancer Res. 2006;12(4):1317-1324.
42. Jain T, Dueck AC, Kosiorek HE, et al. Phase II trial of nab-paclitaxel in patients with relapsed or refractory multiple myeloma. Am J Hematol. 2016;91(12):E504-E505.
43. Takaoka A, Hayakawa S, Yanai H, et al. Integration of interferon-alpha/beta signalling to p53 responses in tumour suppression and antiviral defence. Nature. 2003;424(6948):516-523.
44. Thyrell L, Erickson S, Zhivotovsky B, et al. Mechanisms of interferon-alpha induced apoptosis in malignant cells. Oncogene. 2002;21(8):1251-1262.
45. Prchal M, Pilz A, Simma O, et al. Type I interferons as mediators of immune adjuvants for T- and B cell-dependent acquired immunity. Vaccine. 2009;27 Suppl 6:G17-20.
46. Tough DF, Kamath AT. Interferon with dendritic cells? Nat Immunol. 2001;2(12):1098-1100.
47. Tudor D, Riffault S, Carrat C, Lefevre F, Bernoin M, Charley B. Type I IFN modulates the immune response induced by DNA vaccination to pseudorabies virus glycoprotein C. Virology. 2001;286(1):197-205.
48. Bergsagel DE, Sprague CC, Austin C, Griffith KM. Evaluation of new chemotherapeutic agents in the treatment of multiple myeloma. IV. L-Phenylalanine mustard (NSC-8806). Cancer Chemother Rep. 1962;21:87-99.
49. Cottini F, Hideshima T, Suzuki R, et al. Synthetic lethal approaches exploiting DNA damage in aggressive myeloma. Cancer Discov. 2015;5(9):972-987.
50. Neri P, Ren L, Gratton K, et al. Bortezomib-induced "BRCAness" sensitizes multiple myeloma cells to PARP inhibitors. Blood. 2011;118(24):6368-6379.
51. Hanamura I, Stewart JP, Huang Y, et al. Frequent gain of chromosome band 1q21 in plasma-cell dyscrasias detected by fluorescence in situ hybridization: incidence increases from MGUS to relapsed myeloma and is related to prognosis and disease progression following tandem stem-cell transplantation. Blood. 2006;108(5):1724-1732.